Journal of Applied Electrochemistry (2007) 37:315–324
DOI 10.1007/s10800-006-9259-z

Calculation of temperature transients in pulse electrochemical machining (PECM)

N. SMETS*, S. VAN DAMME, D. DE WILDE, G. WEYNS and J. DECONINCK
Vrije Universiteit Brussel IR/ETEC, Pleinlaan 2, 1050, Brussels, Belgium
*(*author for correspondence, E-mail: nsmets@vub.ac.be)*

Received 12 May 2006; accepted in revised form 10 October 2006

Key words: pulse electrochemical machining, simulations, temperature distribution, thermal boundary layer, time scales, transient

Abstract

Pulse Electrochemical Machining (PECM) is a manufacturing process which provides an economical and effective method for machining hard materials into complex shapes. One important drawback of ECM is the lack of quantitative simulation software to predict the tool shape and machining parameters necessary to produce a given work-piece profile. Calculating temperature distributions in the system allows more accurate simulations, as well as the determination of the thermal limits of the system. In this paper temperature transients over multiple pulses are calculated. It is found that the way the system is modeled has a great impact on the temperature evolution in the thermal boundary layer. The presence of massive electrodes introduces extra time scales which may not be negligible. It is advantageous to identify the thermal time scales in the system, to see whether the heat produced during separate pulses will accumulate or not during the process. The occurring thermal time scales in the system are discussed in detail.

List of Symbols

a	Polarization parameter 1/S m^{-2}
A	Electrode surface/m^2
b	Polarization parameter 2/A m^{-2}
Bi	Biot number/–
C_p	Heat capacity/J kg^{-1} K^{-1}
$D_{0,i}$	Diffusion coefficients at infinite dilution/ m^2 s^{-1}
E_0	Equilibrium potential/V
Fo	Fourier number/–
h	Heat transfer coefficient/W m^{-2} K^{-1}
H	Characteristic size electrode/m
I	Electrical current/A
J	Current density distribution/A m^{-2}
k	Thermal conductivity/W m^{-1} K^{-1}
k_{mol}	Molecular thermal conductivity/ W m^{-1} K^{-1}
k_{turb}	Turbulent thermal conductivity/ W m^{-1} K^{-1}
L	Electrode length/m
$P_{doublelayer}$	Heat produced in the double layer/W m^{-2}
P_{bulk}	Heat produced in the bulk/W m^{-3}
Pr_t	Turbulent Prandtl number/–
q	Heat/W
St_0	Strouhal number/–
St_0	Strouhal number for flushing period/–
t	Time/s
t_0	Pulse off-time/s
T	Pulse period/s
Δt_c	Transient duration due to convection/s
U	Potential distribution/V
ν	Scalar velocity/m s^{-1}
$\bar{v}$	Velocity vector/m s^{-1}
V	Volume/m^2
x	Distance/m
α	Duty cycle/–
α'	Thermal diffusivity/m^2 s^{-1}
η	Overpotential/V
θ	Relative temperature/K
θ'	Normalized temperature/K
Θ	Temperature/K
Θ_i	Initial temperature/K
Θ_∞	Reference temperature/K
$\hat{\lambda}_n$	Transcendental coefficients/–
μ	Dynamic viscosity/kg m^{-1} s^{-1}
ρ	Density/kg m^{-3}
σ	Electrical conductivity/S m^{-1}
τ	Time constant/s

1. Introduction

Electrochemical Machining (ECM) is a manufacturing process based on the controlled anodic dissolution of a metal at large current densities (in the range of 1 A mm^{-2}. An electrolytic cell is created in which the tool (cathode) is advanced towards the work-piece (anode). The electrolyte is pumped through the electrode

gap at high speed to carry away reaction products, heat and gas.

When it comes to the machining of components of complex geometry and hard material, ECM has some obvious advantages over conventional milling or turning procedures: it can be applied regardless of material hardness, there is no tool wear and a high quality surface can be obtained with no residual stresses or damage to the microstructure [1–3]. Accordingly, many high quality parts are produced using ECM, from shaver heads to turbine blades.

Despite its advantages, some difficulties still trouble the application of ECM. One important issue is the lack of quantitative simulation software to predict the tool shape and machining parameters necessary to produce a given work-piece profile [3–5]. The most complete model needs to deal with the effects of the fluid flow, gas evolution, heat generation, the electrochemical processes at the electrodes, the transport of the species involved and the electrode shape change. This work makes a contribution in incorporating the heat generation in the model, and calculating the temperature distributions.

Pulse Electrochemical Machining (PECM) involves the application of current or voltage pulses. In this work only current pulses will be considered. This does not compromise the generality, since voltage and current are closely related. One wishes to apply pulsed current for reasons of accuracy and surface quality [3, 6–8]. The application of pulsed current can also reduce the thermal load on the work-piece, while still maintaining the desired current density during the pulse on-time. The issue of heating of the electrolyte is of primary importance for the determination of the limit conditions in ECM [6, 7, 9–11].

Steady state temperature distribution calculations have been performed by Clark and McGeough [9], Loutrel and Cook [11] and Kozak et al. [10]. Time accurate calculations of temperature distribution during PECM have already been performed by Kozak [7, 8]. In [8] no heat flux into the electrodes is considered. In [7] heat flux into the electrodes is considered, but by applying fixed temperatures on the electrodes, Kozak considers the electrode and its thermal conductivity to be infinitely large. In [7, 8] the pulses are considered to be independent, and thus no accumulation of heat over multiple periods is encountered. In this work the electrodes are modeled as massive lumps with finite dimensions, which introduces extra time scales in the system. The time scales are studied, and used to see whether the separate pulses can be considered independent or not. Temperature transients over multiple periods can be calculated.

2. Mathematical model

The full electrochemical model used in this work, is described in a separate paper [12]. In this paper mainly the thermal aspects are considered.

In order to find the local flow field the incompressible Reynolds averaged Navier–Stokes (RANS) equations are solved. The turbulent viscosity which enters these equations, is calculated using the low-Re k–ω turbulence model. A detailed description of the equations, the boundary conditions and the numerical solution techniques can be found in [13].

The excess supporting electrolyte means that the potential distribution U in the electrolyte is governed by the Laplace equation

$$\overline{\nabla}.\left(\sigma\overline{\nabla}U\right) = 0 \tag{1}$$

with non linear boundary conditions due to the electrochemical reactions. The electrical conductivity σ, is a function of ionic concentrations, which is extensively treated in [12]. σ is also a function of the temperature Θ. The diffusion coefficients at infinite dilution $D_{0,i}$, used to calculate the conductivity [12], are multiplied with a factor $[1 + 0.02(\Theta-\Theta_\infty)]$ to increase the coefficients 2% per Kelvin.

The local current density J can be calculated using

$$\bar{J} = -\sigma\overline{\nabla}U. \tag{2}$$

A linearized overpotential is used to model the polarization on the surface of the electrodes,

$$J = a(U_{electrode} - U_{\text{electrolyte}}) + b. \tag{3}$$

According to

$$U_{\text{electrode}} - U_{\text{electrolyte}} = \eta + E_0 \tag{4}$$

the potential difference over the double layer is composed of an equilibrium potential E_0 and an overpotential η. The equilibrium potential is deliberately assumed to be zero, to facilitate calculations. Without compromising the generality, Equation (3) then yields

$$J = a\eta + b. \tag{5}$$

The current efficiency on the anode, where the electrochemical dissolution of the metal takes place, is assumed to be 100%, so no current is consumed by the production of oxygen gas.

It is considered that in this system (also used in [12]), two ions strongly influence the local conductivity, σ, namely iron ions at the anode and hydroxide ions at the cathode. The ion production at the electrodes is calculated from the local current density. The ion distributions are calculated using convection–diffusion equations with mass fluxes on the boundaries [12].

The temperature distribution in the system is calculated using a convection–diffusion equation with heat sources, as shown in Equation (6).

$$\rho C_{\text{p}}\frac{\partial\Theta}{\partial t} + \rho C_{\text{p}}\bar{v}.\overline{\nabla}\Theta = \overline{\nabla}.(k\overline{\nabla}\Theta) + P_{\text{bulk}} \tag{6}$$

The thermal conductivity k is composed of the molecular thermal conductivity k_{mol} and the turbulent thermal conductivity k_{turb}, as shown in Equation (7).

$$k = k_{\mathrm{mol}} + k_{\mathrm{turb}} \tag{7}$$

Joule heating in the bulk of both the electrolyte and the electrodes is considered, where

$$P_{\mathrm{bulk}} = \frac{J^2}{\sigma}. \tag{8}$$

Heat dissipation in the double layer, where [11]

$$P_{\mathrm{doublelayer}} = \eta J, \tag{9}$$

is also taken into account. $P_{\mathrm{doublelayer}}$ is imposed as heat flux at the boundaries of the domains. The boundaries of the electrodes, which are not contiguous to the electrolyte, are considered thermal insulators. This choice is justified by the fact that essentially all of the heat generated in the system must be carried away by the electrolyte [11].

3. Implementation

All partial differential equations presented above were solved in two spatial dimensions (2D) using the residual distribution method [14]. The scalar N-scheme was applied to the convective terms in the convection–diffusion equations. Equal distribution was applied to the diffusion terms. All numerical schemes provided at least second order accuracy [15]. An implicit second order – time accurate – time integration scheme was used [16, 17].

4. Numerical simulations: results and discussion

The following general data were used in the calculations. For the calculation of the flow field, the dynamic viscosity $\mu = 0.001$ kg m^{-1} s^{-1}, the electrolyte density $\rho_{\mathrm{electrolyte}} = 1000$ kg m^{-3} and the average flow velocity $v_{av} = 15$ m s^{-1}. The flow was fully developed at the channel inlet.

The linearized overpotentials for the anode and the cathode were respectively $J_{\mathrm{anode}} = 0.33 \times 10^6$ S m^{-2} $\eta - 0.76 \times 10^6$ A m^{-2} and $J_{\mathrm{cathode}} = 10 \times 10^6$ S m^{-2} $\eta + 10 \times 10^6$ A m^{-2}. These polarization values were taken from the work of Van Damme et al. [12], who obtained the experimental data from [18]. The equilibrium potential E_0 was however not included in the measurements, and is by default set equal to zero. This does not compromise the general principles shown in this work. The electrical conductivity of the electrolyte at the inlet of the flow channel was $\sigma = 16.485$ S m^{-1}, the electrical conductivity of the electrodes was $\sigma = 10^6$ S m^{-1}. For the electrolyte $\rho C_p = 4.17 \times 10^6$ J m^{-3} K^{-1} and $k_{\mathrm{electrolyte}} = 0.5984$ W m^{-1} K^{-1}. For the electrodes $\rho C_p = 3.55 \times 10^6$ J m^{-3} K^{-1} and $k_{\mathrm{electrode}} = 81$ W m^{-1} K^{-1}. The electrolyte temperature was $\Theta_\infty = 20$ °C $= 293.15$ K at the inlet. For the turbulent Prandtl number the typical value $Pr_t = 0.71$ was taken [19].

The duty cycle α is the ratio of the pulse on-time to the total period T of the pulse. In this work, $\alpha = 10\%$ for all the simulations. All the simulations in this paper were performed on simple channels with rectangular electrodes. The shown temperature evolutions θ are all relative to the electrolyte temperature Θ_∞.

$$\theta = \Theta - \Theta_\infty \tag{10}$$

The meshes assured grid convergence and the smallest mesh elements in the flow channel on the electrode surfaces were 10^{-7} m in height in order to capture the thermal boundary layer in detail.

4.1. *Channel with infinitely thin electrodes*

The first geometry studied was a simple channel without physical electrode domains. The electrodes were infinitely thin and did not accumulate heat. The electrodes had a length of $L = 3$ mm. The channel was 200 μm in height and the depth (along the Z dimension) was 10 mm. The surface of the electrodes was $A = 30$ mm^2. The applied current during the on-time of the pulses was $I_{\mathrm{pulse}} = 30$ A, so that the average current density during the on-time was $J_{\mathrm{pulse}} = 1$ A mm^{-2}. The calculated temperature fields were two dimensional and function of time. This provided too much information to display in this paper, hence the temperature was probed from six reference points A, B, C and D, E, F and plotted as a function of time. A was located at the end of the anode (downstream), B in the middle of the anode, and C in the middle at a distance of 2.4 μm from the anode, see Figure 1. The electrolyte flowed from left to right. The three other reference points D, E and F were located in the center of the flow channel, respectively at the start, at the middle and at the end of the electrodes, as is shown in Figure 2.

Most of the heat in this system was generated in the double layers. This heat was removed by convection by the electrolyte. A thermal boundary layer was formed. Figure 1 shows the thermal boundary layer at steady state at the anode when a constant current of 30 A was applied.

When applying current pulses, heat is generated only during the on-time. If the off-time of the pulses is long

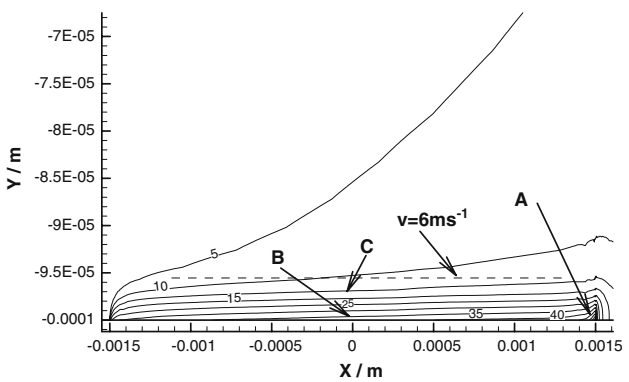

Fig. 1. Zoom on the thermal boundary layer at steady state ($I = 30$ A) at the anode. Lines of equal temperature θ are shown. Also showing reference points A, B and C.

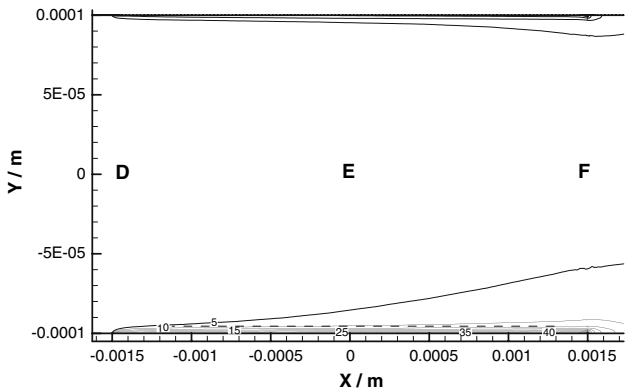

Fig. 2. Whole flow channel, showing the temperature field at steady state (I = 30 A). Lines of equal temperature θ are shown. Also showing reference points D, E and F.

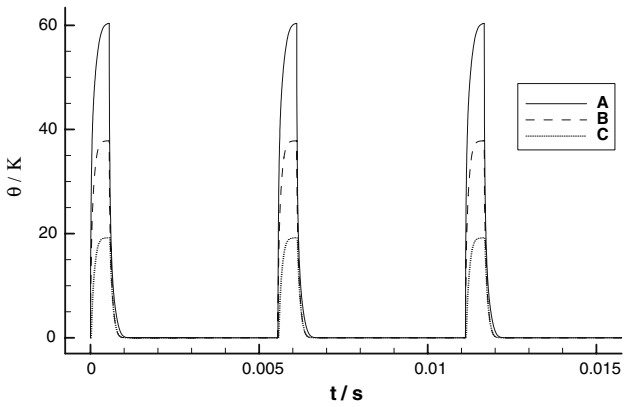

Fig. 3. Temperature evolutions in reference points A, B and C for a local St_0 = 0.1. Geometry with infinitely thin electrodes.

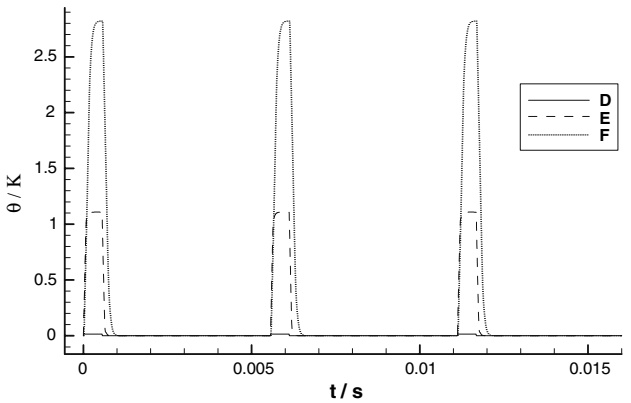

Fig. 4. Temperature evolutions in reference points D, E and F for a local St_0 = 0.03. Geometry with infinitely thin electrodes.

enough, all the heat produced in the system is flushed away by the electrolyte. In case of such total flushing, all the pulses can be considered independent of each other, and the analysis of a single pulse can be applied to multiple pulses. If convection is dominant over diffusion, which is mostly the case in ECM because of the high electrolyte flow velocities, the Strouhal number can be used to quantify whether the pulses can be considered independent of each other or not. The Strouhal number is defined as $St = L/\nu t$. The Strouhal number for the flushing period St_0 [6–8] is

$$St_0 = \frac{L}{\nu t_0}, \tag{11}$$

where $t_0 = (1-\alpha)T$. The Strouhal number for the flushing period will be referred to as the Strouhal number for the rest of the paper.

If $St_0 \ll 1$, $\nu t_0 \gg L$, which means that the heat is convected much further than an electrode length L during the off-time t_0. The residence time of the heat in the system is relatively limited and total flushing will occur. A calculation was performed with St_0 = 0.1 in the thermal boundary layer. The calculations show that the thermal boundary layer is much thinner than the hydrodynamic boundary layer, and hence the velocity of the electrolyte removing the heat, is considerably lower than the average electrolyte velocity. The velocity was chosen somewhere in the middle of the thermal boundary layer in steady state (see Figure 1), where the RANS equations yielded ν = 6 m s^{-1}. A period T = 5.56 ms yields a Strouhal number St_0 = 0.1 in the thermal boundary layer. The Strouhal number in the center of the channel is lower (0.03), because the electrolyte velocity is higher (18.9 m s^{-1}). The temperature evolutions in the reference points A, B, C and D, E, F are shown respectively in Figures 3 and 4. It is clear that the heat is completely removed during the off-time of the pulse, and the pulses can be considered independent of each other. At the start of a pulse on-time and off-time a short transient is noticeable, which takes about 500 μs for reference point A and 300 μs for reference points B and C. In the center of the channel the transient duration varies from about 9 μs in D, 100 μs in E to 300 μs in F.

A period T = 556 μs yields a Strouhal number St_0 = 1 in the thermal boundary layer. If St_0 = 1, $\nu t_0 = L$. The temperature evolutions in the reference points A, B and C are shown in Figure 5. The flushing time is just sufficient to remove all the heat accumulated in the thermal boundary layer, making the next pulse independent of the previous. As in Figure 3, also

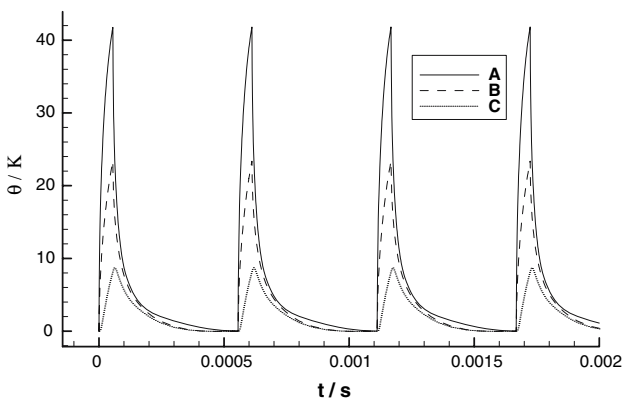

Fig. 5. Temperature evolutions in reference points A, B and C for a local St_0 = 1. Geometry with infinitely thin electrodes.

in Figure 5 the transient takes about 500 μs in reference point A, and about 300 μs in reference points B and C in the thermal boundary layer. The temperature evolutions in the reference points D, E and F in the center of the channel, where $St_0 = 0.3$, show no new behaviour compared to the previous case (Figure 4) and the single pulses are still very independent of each other.

If St_0 is large, $vt_0 \ll L$, the heat will travel only a fraction of the electrode length L during the off-time t_0. The flushing during the off-time will be very poor. A period $T = 55.6$ μs yields a Strouhal number $St_0 = 10$ in the thermal boundary layer. The temperature evolutions in the reference points A, B and C are shown in Figure 6. Heat will accumulate during several periods, giving rise to a long transient in the temperature evolution of about 500 μs for reference point A and about 300 μs for reference points B and C. The temperature evolutions in the reference points D, E and F, where $St_0 = 3$, are shown in Figure 7. Also here slow transients are noticeable, with the same durations as found earlier for reference points D, E and F, respectively about 9, 100 and 300 μs.

4.2. *Channel with massive electrodes*

4.2.1. *Geometry 1*

The same geometry as in Section 4.1 was used here, extended with physical electrode domains. The electrodes were 3 mm in length, 200 μm in height, and 10 mm in depth along the Z-axis. The reference points A, B, C and D, E, F were preserved as in Figures 1 and 2, and two extra reference points G and H were chosen in the anode, as shown in Figure 8.

When current pulses with a period of $T = 5.56$ ms were applied, which yielded a Strouhal number $St_0 = 0.1$ in the thermal boundary layer, the temperature evolutions for reference points A, B, C and G, H in Figure 9 were obtained. The temperature evolutions are very different from those in Figure 3. The temperature rise during the on-time of the pulse is less steep with the massive electrode present, resulting in much lower temperature peaks. The temperature drop during the off-time of the pulse is also less pronounced. It can also be seen from Figure 9 that there is a transient of several pulse periods, even though the Strouhal number is low. We conclude that even a very thin electrode has a large

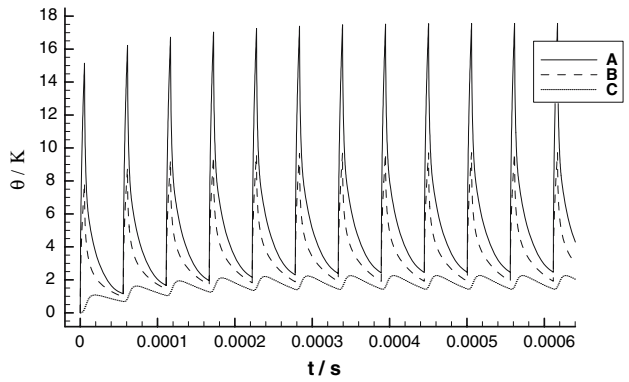

Fig. 6. Temperature evolutions in reference points A, B and C for a local $St_0 = 10$. Geometry with infinitely thin electrodes.

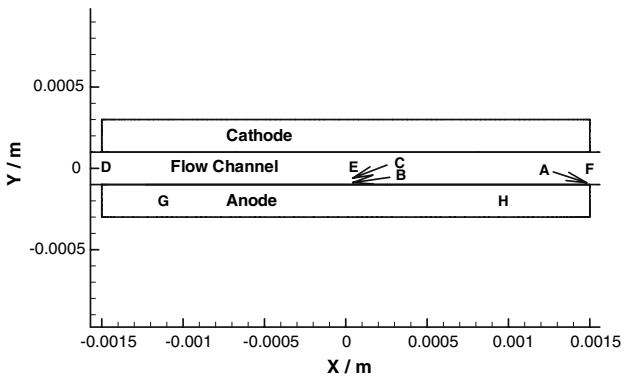

Fig. 8. Geometry with a massive anode of 200 μm high. Reference points G and H added.

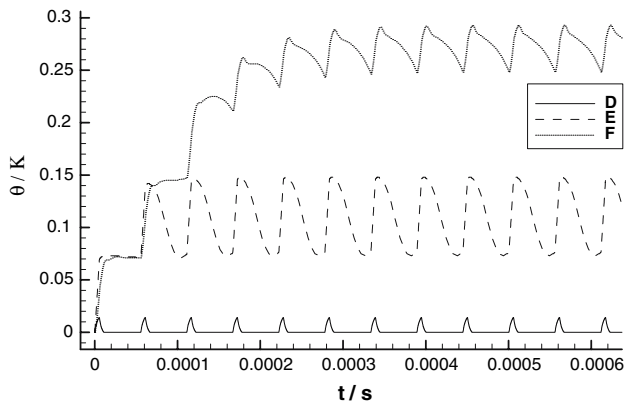

Fig. 7. Temperature evolutions in reference points D, E and F for a local $St_0 = 3$. Geometry with infinitely thin electrodes.

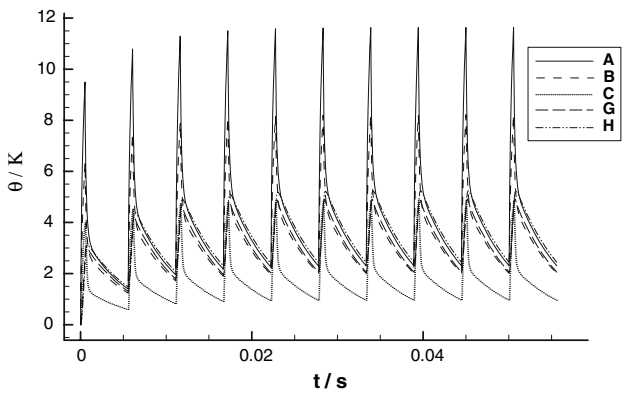

Fig. 9. Temperature evolutions in reference points A, B, C and G, H for a local $St_0 = 0.1$. Geometry with a massive anode of 200 μm high.

impact on the temperature evolution in the thermal boundary layer. Two time scales can be observed in the temperature evolutions in Figure 9. For reference points A, B and C the temperature drops relatively fast in the beginning of the off-time, but short thereafter the temperature starts to drop much slower. The phenomenon is more pronounced during the off-time, but as will be shown later, is also present during the on-time. For reference points G and H the temperature evolution is more uniformly varying.

The temperature evolutions in reference points D, E and F in the center of the flow channel, where $St_0 = 0.03$ are shown in Figure 10. Also here two time scales are noticeable. The temperature evolution is very fast in the beginning, but slows down significantly afterwards. A remark has to be made that, in Figure 10, there is a very weak slow transient present, as in Figure 9. This transient is however so minor that it can be neglected.

An explanation for the observed phenomenon will be given in the following. If the temperature of the electrode and electrolyte is not the same there will logically be heat transport between these two. Hence the presence of the electrode in the system will be accompanied by the permanent presence of a thermal boundary layer. During the on-time of the pulse much of the produced heat will flow in the electrode. This electrode acts as a buffer and whole or part of the accumulated heat will be carried away by the electrolyte during the off-time afterwards. This explains the lower temperature peaks, and the slow transient that can be observed. Two time scales can be noticed in the temperature evolutions. The first, and in this case the fastest, is the transient duration for the convective transport. During the off-time this means that it takes some time to flush the channel with fresh electrolyte, causing a gradual drop in temperature. The second time scale, in this case the slower one, is due to the presence of the electrode. The buffered heat flows out of the electrode during the off-time giving rise to a thermal boundary layer with similar dynamic behaviour as the electrode. If the channel is flushed by convection, this causes a strong drop in temperature. Afterwards, the temperature evolution is controlled by the thermal boundary layer, causing the slower temperature dropping in Figure 9 for reference points A, B and C, and in Figure 10 for reference point F. For reference points G and H (Figure 9) only the time scale of the electrode is present, since there is no convection.

In the electrolyte, it is not only the Strouhal criterion that shows whether the heat produced by multiple pulses will accumulate or not. The presence of a massive electrode introduces new thermal dynamics in the thermal boundary layer.

It has to be noted that in turbulent flow conditions the thermal boundary layer rapidly increases in thickness due to the high turbulent heat diffusivity (see Figure 2), and can easily fill up the whole channel after a certain distance. Hence the influence of the thermal boundary layer can be very significant. In case of significant heating in the double layer, the thermal boundary layer gains in importance.

A calculation with pulse period $T = 1.85$ ms ($St_0 = 0.3$ in the thermal boundary layer) was performed. The temperature evolutions in the reference points A, B, C and G, H are shown in Figure 11. The temperature evolutions in the reference points D, E and F, with a local Strouhal number of $St_0 = 0.1$, are analogous to the previous case with a local Strouhal number $St_0 = 0.03$ (see Figure 10), and are not shown.

4.2.2. *Geometry 2*

The same geometry as in Section 4.2.1, but with an anode with a height of 3 mm, was used in this section. The reference points A, B, C and D, E, F were again preserved. The reference points G and H were chosen as shown in Figure 12.

Applying a pulsed current with a period of $T = 0.1$ s ($St_0 = 0.006$ in the thermal boundary layer) produced the temperature evolutions in the reference points A, B, C and G, H as shown in Figure 13. The temperature evolutions in reference points D, E and F ($St_0 = 0.002$) are shown in Figure 14. The same observations as in Section 4.2.1 can be made. The temperature evolutions

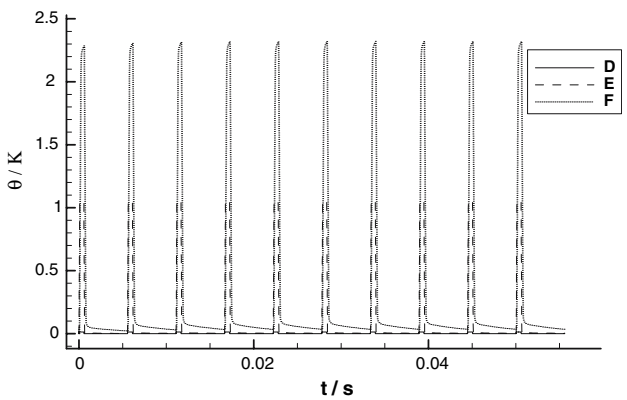

Fig. 10. Temperature evolutions in reference points D, E and F for a local $St_0 = 0.03$. Geometry with a massive anode of 200 μm high.

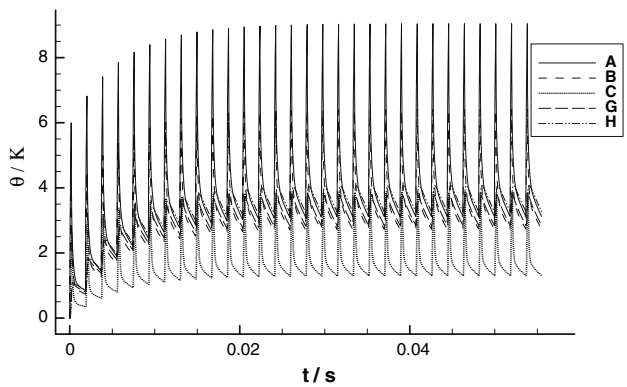

Fig. 11. Temperature evolutions in reference points A, B, C and G, H for a local $St_0 = 0.3$. Geometry with a massive anode of 200 μm high.

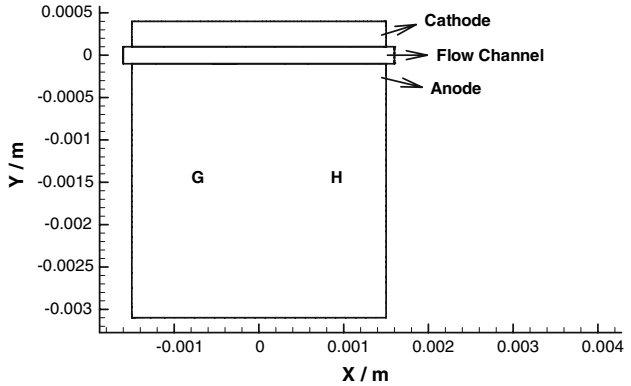

Fig. 12. Geometry with a massive anode of 3 mm high.

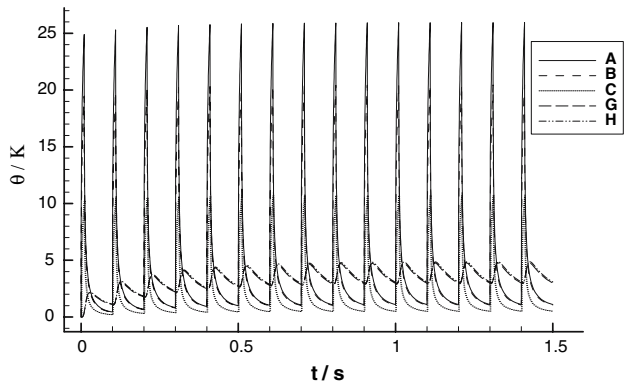

Fig. 13. Temperature evolutions in reference points A, B, C and G, H for $T = 0.1$ s ($St_0 = 0.006$). Geometry with a massive anode of 3 mm high.

in Figure 13 contain a slow transient, and 2 time scales can be observed in the ripple for reference points A, B and C. In Figure 14 the slow transient is negligible. The two time scales are very well visible during both the on and off-times of the pulses. The two time scales are orders of magnitude different from each other, and in order to capture them both accurately the time grid is very dense at the start of a pulse on- and off-time.

If the pulse period T is many orders of magnitude smaller than the largest thermal time scale in the system, a large amount of timesteps have to be calculated to get the detailed transient. This is a very computationally expensive procedure, and will be the subject of future work.

4.2.3. *Analytical solutions*

Two time scales are observed in the system. First, there is a transient from the convective transport, and second there is a time constant from the thermal dynamics of the electrode. These time scales can be estimated analytically. The software used in this paper has also been validated using these analytical models under their limited conditions.

4.2.3.1. Convective transport transient. The first transient encountered is caused by the convective transport. If only convection and heating is considered and the problem is reduced to 1 dimension (1D), Equation (6) simplifies to a transport equation with a source

$$v\frac{\partial\theta}{\partial x}+\frac{\partial\theta}{\partial t}=\frac{P_{\text{bulk}}}{\rho C_{\text{p}}}=P^{*}, \tag{12}$$

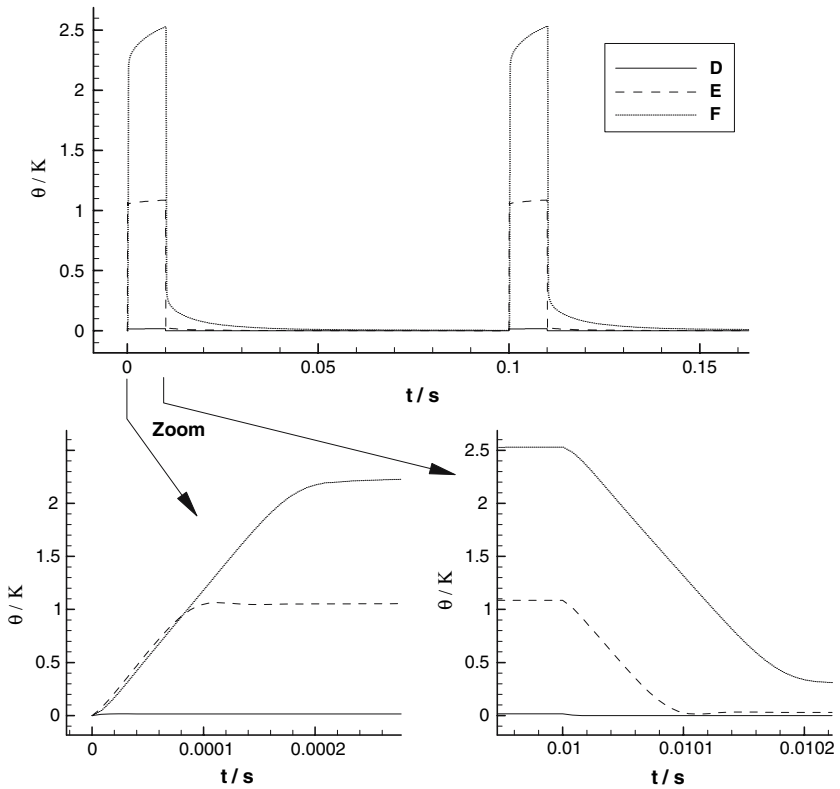

Fig. 14. Temperature evolutions in reference points D, E and F for $T = 0.1$ s ($St_0 = 0.002$). Geometry with a massive anode of 3 mm high.

where relative temperatures are used, see Equation (10). The solution $\theta(x,t)$ in the flow channel is the surface tangent to the (constant) characteristic direction vector $(v,1,P^*)$ in the (x,t,θ) space, according to [20]. Obeying the initial condition $\theta(x,0) = 0$ and the boundary condition $\theta(0,t) = 0$, the solution in the flow channel is graphically shown in Figure 15. For a certain point in space where $x = \Delta x$, the temperature will rise linearly with time in the beginning, and becomes constant (steady state) when the characteristic direction is crossed. The transient duration Δt_c is then

$$\Delta t_c = \frac{\Delta x}{v}. \tag{13}$$

Δt_c equals the time the electrolyte needs to pass from the beginning of the channel to the point where $x = \Delta x$. Note that this is analogous to the case where the Strouhal number equals one.

In the case with infinitely thin electrodes, at the end of the flow channel (reference point A) in the thermal boundary layer we find $\Delta t_c = 500$ μs. Halfway of the flow channel (reference points B and C) in the thermal boundary layer we find $\Delta t_c = 250$ μs. These are indeed more are less the transient durations found in Figures 3, 5 and 6.

In the center of the flow channel we can calculate for reference points D, E and F respectively $\Delta t_{c,D} = 0$ μs, $\Delta t_{c,E} = 80$ μs, $\Delta t_{c,F} = 160$ μs. These transient durations are found back in Figures 4, 7, 10 and 14. The linear evolution is also very present.

4.2.3.2. Thermal time constant of the electrode. The temperature evolution in the electrode has a large impact on the temperature evolution in the thermal boundary layer in the electrolyte. The thermal behaviour of the electrodes during the PECM process can be approximated using analytical solutions. These analytical solutions are only valid under limited conditions, but they can provide interesting information.

If the assumption is valid that the whole electrode is always at a uniform temperature $\Theta_{electrode} = \Theta(t)$, a lumped capacity solution can be used. This assumption is valid if the Biot number [21] is much smaller than one

$$Bi = \frac{hH}{k} \ll 1, \tag{14}$$

for which $H = V/A$ will be taken.

Heat $q(t)$ will be produced at the surface of the electrode. Part of this heat will be removed by the electrolyte: $q_{convection}$, and the other part will heat up the electrode: $q_{electrode}$.

In Figure 16 a schematic is drawn, with the electrolyte and its characteristics in the upper half, and the electrode and its characteristics in the lower half.

The following system of equations applies

$$\begin{cases} q_{convection} = hA(\Theta(t) - \Theta_\infty) \\ q_{electrode} = \rho C_p V \dfrac{d\Theta(t)}{dt} \\ q_{convection} + q_{electrode} = q \end{cases} \tag{15}$$

with initial condition

$$\Theta(0) - \Theta_\infty = \theta_{start}. \tag{16}$$

The solution of the system of Equations (15), (16) and (10) is

$$\theta(t) = \theta^* - (\theta^* - \theta_{start})e^{-\frac{t}{\tau}} \tag{17}$$

with time constant $\tau = \rho\, C_p\, H/h$, and with $\theta^* = q/hA$.

Equation (17) shows that the temperature variation is exponential. During the on-time of the pulse, the temperature rises exponentially, and during the off-time of the pulse ($q = 0$ and hence $\theta^* = 0$) the temperature drops exponentially.

For the geometry in Section 4.2.1, the FEM calculations yield an average heat transfer coefficient $h = 134$ kW m^{-2} K^{-1} and thus $Bi = 0.33$. The time constant of the lumped capacity solution then yields $\tau = 5.30$ ms. The temperature evolutions of the up and down slopes in Figures 9 and 11 are, however, not simple exponentials, since the convection transient is also present. A curve fitting yields that the time constant of the slow transient in Figures 9 and 11 is $\tau_{fit} = 5.96$ ms, which is very close to the theoretically obtained value. The total slow transient takes about 5τ.

In ECM the flow velocities are typically relatively high, giving rise to high convection coefficients h, and hence, high Bi numbers. In such cases the lumped capacity solution is not valid. The transient conduction in a 1D slab is described in the literature. If the slab is

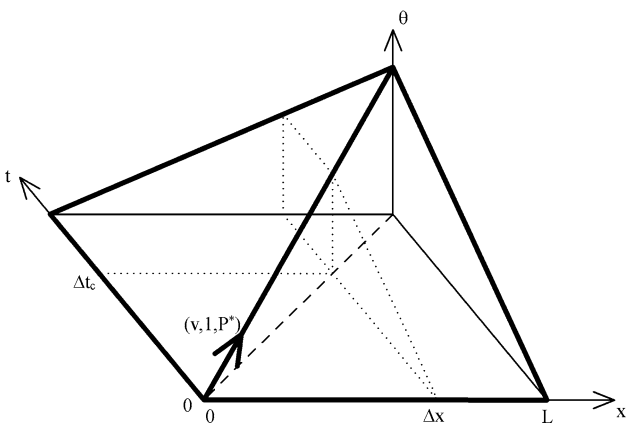

Fig. 15. Graphical solution of the transport equation with heat source.

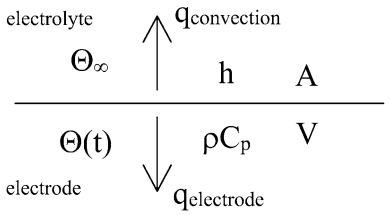

Fig. 16. Schematic of the lumped capacity solution.

cooled by convection with a constant convection coefficient h the solution is [21]

$$\theta' = \sum_{n=1}^{\infty} e^{-\hat{\lambda}_n^2 Fo} \frac{2\sin\hat{\lambda}_n}{\hat{\lambda}_n + \sin\hat{\lambda}_n \cos\hat{\lambda}_n} \cos(\hat{\lambda}_n \frac{x}{H}) \quad (18)$$

where $Fo = \alpha' t/H^2$ and $\alpha' = k/\rho\, C_p$. Starting from the side which is not cooled the distance x is measured and $\theta' = (\Theta - \Theta_\infty)/(\Theta_i - \Theta_\infty)$. The coefficients $\hat{\lambda}_n$ are the successive roots of the transcendental equation

$$\cot\hat{\lambda}_n = \frac{\hat{\lambda}_n}{Bi}. \quad (19)$$

The graphical representation of Equation (18) can be seen in the Heisler charts for $0 \leq Fo \leq 1.5$ [21]. The temperature evolution during the cooling of the electrode during the off-time of the pulse can be read from these charts.

For $Fo > 0.2$ the series from Equation (18) may be approximated using only their first term

$$\theta' \approx A_1 \cos(\hat{\lambda}_1 \frac{x}{H}) e^{-\hat{\lambda}_1^2 Fo} \quad (20)$$

with A_1 and $\hat{\lambda}_1$ tabulated as a function of the Biot number [21].

For the geometry in Section 4.2.2, the FEM calculations yield an average heat transfer coefficient $h = 136\ \mathrm{kW\ m^{-2}\ K^{-1}}$ and thus $Bi = 5$. The time constant in Equation (20) yields $\tau = H^2/\alpha'\hat{\lambda}_1^2 = 229$ ms. Again here, the temperature slopes during the on and off-times of the pulses are not simple exponentials. In this case the convection transient is very short, and thus does not hamper the analysis of the temperature evolution due to the dynamic behaviour of the electrode. The temperature evolutions are not simple exponentials because $Fo < 0.2$ and hence the analytical solution is a sum of multiple exponentials with different time constants (see Equation (18)). Added to this, the initial temperature field before cooling down or warming up can be far from uniform in the numerical simulation, while it is an assumption used for the analytical solution. For the slow transient the time constant can be estimated however. Curve fitting gives the time constant of the slow transient in Figure 13 as $\tau_{fit} = 221$ ms, which is very close to the theoretically obtained value.

5. Conclusions

Thermal calculations in electrochemical systems under pulsed current conditions have been performed. The main difference from previous work is that massive electrodes are incorporated as physical domains in the modeling. The electrodes can have a large impact on the thermal evolution in the electrolyte thermal boundary layer, and hence on the final shape change of the electrode surface. Also calculations can be performed over several periods, providing the opportunity to simulate slow transients in the temperature evolution during multiple periods, and thus providing a simulation tool for the determination of the thermal limits of the system under high machining rate conditions.

Multiple time scales are encountered in the system. Studying the time scales allows us to determine in advance, whether the heat produced by different pulses will accumulate over time. A first time scale in the system is caused by the transient of the convective transport. This time scale is encountered in the whole flow channel.

If a massive electrode is added to the thermal system, it acts as a buffer, limiting the slopes of the temperature evolution, and receiving and giving heat. This introduces a new thermal time constant, which governs the dynamics of the thermal boundary layer. This thermal boundary layer is restricted in space, and diminishes further away from the electrode interface.

Locally one has to consider the slowest phenomenon to determine whether the heat will accumulate during multiple pulses or not. In the bulk of the electrolyte, far enough from the thermal boundary layers, only the convection transient is encountered. The influence of the electrodes is too far away, and hence the Strouhal number St_0 qualifies as a valid criterion as to whether total flushing occurs during the pulse off-time or not.

Near the wall the influence of the thermal boundary layer is considerably large. Because the time scale of the electrodes is the largest in the cases in this work, the Strouhal criterion is no longer valid here. Instead it is the thermal dynamic behaviour of the electrode that determines whether total flushing will occur during the pulse off-time or not.

It is shown that the analytical models are too limited for determining the temperature evolution during the alternating on and off-times of the pulses. The analytical models can, however, be useful to approximate the time scales encountered in the system during PECM, as shown in this work.

References

1. D. Risco and A. Davydov, *J. Am. Soc. Mech. Eng.* **64** (1993) 701.
2. J. McGeough, *Principles of Electrochemical Machining* (J. Wiley & Sons, New York, 1974).
3. K.P. Rajurkar, D. Zhu, J.A. McGeough, J. Kozak and A. De Silva, *Ann. CIRP* **48**(2) (1999) 567.
4. M. Lohrengel, I. Kluppel, C. Rosenkranz, H. Betterman and J. Schultze, *Electrochim. Acta* **48**(20–22) (2003) 3203.
5. A. Mount, D. Clifton, P. Howarth and A. Sherlock, *J. Mater. Process.Technol.* **138** (2003) 449.
6. M. Datta and D. Landolt, *Electrochim. Acta* **7** (1981) 899.
7. J. Kozak, *Bull. Polish Acad. Sci. Tech. Sci.* **52** (2004) 313.
8. J. Kozak and K. Rajurkar, *J. Mater. Process. Technol.* **28**(1–2) (1991) 149.
9. W. Clark and J. McGeough, *J. Appl. Electrochem.* **7** (1977) 277.
10. J. Kozak, K. Rajurkar and K. Lubkowski, *Trans. NAMRI/SME* **XXV** (1997) 159.
11. S. Loutrel and N. Cook, *ASME J. Eng. Indust.* **95**(B/4) (1973) 1003.
12. S. Van Damme, G. Nelissen, B. Van Den Bossche and J. Deconinck, *J. Appl. Electrochem.* **36**(1) (2006) 1.

13. G. Nelissen, B. Van Den Bossche, J. Deconinck, A. Van Theemsche and C. Dan, *J. Appl. Electrochem.* **33**(10) (2003) 863.
14. G. Nelissen, A. Van Theemsche, C. Dan, B. Van Den Bossche and J. Deconinck, *J. Electroanal. Chem.* **563**(2) (2004) 213.
15. N. Waterson, *Simulation of Turbulent Flow Heat and Mass Transfer Using a Residual-distribution Approach, Dissertation* (Technical University, Delft, 2003).
16. C. Dan, B. Van Den Bossche, L. Bortels, G. Nelissen J. Deconinck, *J. Electroanal. Chem.* **505** (2001) 12.
17. M. Purcar, *Development and Evaluation of Numerical Models and Methods for Electrochemical Machining and Electroforming Applications, Dissertation* (Vrije Universiteit Brussel, Brussels, 2003).
18. H.S.J. Altena, Precision ECM by Process Characteristic Modelling, Dissertation (Glasgow Caledonian University, 2000).
19. G. Nelissen, *Simulation of Multi-ion Transport in Turbulent Flow Dissertation* (Vrije Universiteit Brussel, Brussels, 2003).
20. W.A. Strauss, *Partial Differential Equations: An Introduction* (J. Wiley & Sons, New York, 1992).
21. J.H. Lienhard IV and J.H. Lienhard V, A heat transfer textbook, 3rd edn. (Phlogiston Press, Cambridge, Massachusetts, 2005), pp 762.